IOP Conf. Series: Materials Science and Engineering **230** (2017) 012045 doi:10.1088/1757-899X/230/1/012045

Electrochemical Study of Unmodified and Inhibitor Doped Silane Films for Corrosion Protection of AA2024-T3

Nauman Mubarak, Jin Hu and Shawei Tang
Department of Materials Science and Engineering, Harbin Institute of Technology, Harbin, China
E-mail: naumanmubarak@yahoo.com

Abstract. Aluminum alloy was coated with unmodified and rare-earth inhibitor doped silane films. The role of number of hydrolysable groups, functional group and cerium ions towards film protective quality was investigated. The anti-corrosion performance was evaluated using electrochemical impedance spectroscopy (EIS), d.c. potentiodynamic polarization and energy dispersive x-ray spectroscopy (EDS). The morphology was studied using scanning electron microscopy (SEM). Results indicate improved corrosion protection performance especially for cerium modified silane films with higher number of hydrolysable groups. Inhibitor doped silanes present a facile method for pre-treatment of aluminium alloys prior to deposition of top coat.

1. Introduction

Chromate conversions coatings have been extensively used for corrosion protections of metals such as aluminum and steels [1]. However, hexavalent chromate species are highly carcinogenic and mutagenic in nature and thus, a great amount of recent research has been focused of discovering feasible alternatives [2]. AA2024 is the most widely used aluminum alloy for aerospace applications such as skin for fuselage. This alloy has an inhomogeneous Cu distribution which lends it high strength and improved toughness, but at the same time make it more susceptible to pitting initiation due to increased chances of a galvanic couple being set up between anodic S phase particles like Al2CuMg and the Al matrix. This pitting can then progress due to increased local alkalization resulting from coupled cathodic reactions [3]. The intermetallic particles are also prone to dissolution as the temperature rises and thus degrade the mechanical properties of the alloy. Hence, treatments that try to improve the corrosion resistance of AA2024 alloys should be carried out at temperatures below 120^{o} C [4].

Organofunctional silanes are capable of functionalizing metallic substrates for subsequent polymeric top coat because of the presence of hydrolysable groups that can form a stable bond with substrate and an organofunctional group that can bond with polymer [5]. Silanes can be broadly classified into two categories as mono-silanes and bis-silanes. Mono-silanes have only three hydrolysable groups present at one end of the molecule while the bis-silanes have a total of six hydrolysable groups with three attached to each silicon atom. The presence of a functional group such as amine, marcapto group can also affect the deposition orientation as well as water uptake properties of the silane coatings. Silanes can only provide passive barrier protection, to provide long term enhanced corrosion protection an active system that can repassivate an initial corrosion attack site is required [6]. Rare-earth ions [7], [8] and nanoparticles [9], [10], [11], [12] have been reported as favorable source for providing such an active protection. However, such addition of inhibitors can deteriorate the stability of the sol-gel and lead to an enhanced rate of corrosion [13], [14].

Two different silanes which will incorporate an inhibitor to provide an active corrosion protection were studied. Gamma-amino propyl triethoxysilane (APS) represents a mono-silane with an amine functional group, while bis-trimethoxy silane (BTMS) is a non-functional bis-silane. Inorganic cerium nitrate salt was used as inhibitor ion source.

2. Experiment

2.1. Materials and reagents

Aluminum alloy 2024-T3 was used as the substrate. Strips having dimensions of 4 cm x 8 cm x 0.1 cm were received from Xionglv Metal Material, Dongguan, China. Gamma-Aminopropyl triethoxysilane (99%) and Bis-trimethoxysilane (≥97%) were obtained from Aladdin, Shanghai, China. The silanes were used as received without any further purification. Cerium nitrate hexa-hydrate salt was procured from Guangfu, Tianjin, China. Ethanol, acetone and distilled water were used to clean the substrate samples and to prepare solutions. The pH, where required, was adjusted by using acetic acid.

2.1.1. Coating fabrication

Prior to use, the silanes were functionalized in an alcohol and water solution. The Gamma-Aminopropyl triethoxysilane (APS) solution was prepared by dissolving 5 vol. % of the silane in 90 vol. % ethanol and 5 vol. % distilled water. The Bis-trimethoxysilane (BTMS) solution was prepared by using the same volume ratios. But in this case the pH of the final solution was adjusted to 4 – 4.5 by using acetic acid. The prepared solutions were stirred for 2 hours and then hydrolyzed further for at least 24 hours before use.

The aluminum alloy 2024-T3 strips were ultrasonically cleaned in acetone and ethanol for 15 minutes each. Then rinsed with ample amount of distilled water and blow dried.

2.2. Inhibitor addition and silane treatment

Cerium nitrate hexa-hydrate ($Ce(NO_3)_3.6H_2O$) was selected as a source for the introduction of inorganic ions into the silane films. In order to incorporate these ions a 100 ppm solution of the salt was prepared by dissolving in distilled water. The prepared solution was stirred and heated at 65o C to allow complete solubility of the inhibitor in the water. A 5 vol. % silane solution, was prepared by adding 5 ml of silane and 5 ml of the cerium salt solution to 90 ml of ethanol. The resulting silane inhibitor solution was hydrolyzed by stirring for 2 hours and then allowed to hydrolyze for 48 hours.

The silane films were applied immediately after the alloys strips had been cleaned and dried. The immersion time was between 100-200 seconds at room temperature. The applied films were then cured at 100o C for an hour. This allows to produce adherent films which are extensively cross-liked. This inhibitor loaded coating will be hereafter referred to as Ce-BTMS coating.

2.3. Characterization

The morphology and performance of the silane films was studied using various optical and electrochemical methods. A Hitachi S-3000N machine was used to carry out scanning electron microscopy (SEM) analysis to determine the uniformity and to detect the presence of pin holes in the cured coatings. The operating voltage was 20 kV.

Accelerated corrosion assessment was carried out by performing a DC polarization tests using Princeton Applied Research (PAR) 273-A potentiostat. A three electrode cell was used. The sample was the working electrode. A graphite rod and saturated calomel electrode (SCE) were used as the counter electrode and the reference electrode respectively. A 3.5 wt. % NaCl solution was used as the electrolyte. The samples were immersed for 2 hours in the electrolyte to achieve steady-state conditions. A range of -250mV and +500mV around the Ecorr was used during the experiment. The scan rate was 0.5mV/s.

Thin coatings on substrates have been widely studied by using the electrochemical impedance spectroscopy (EIS) technique. An Autolab 302N potentiostat equipped with Nova software was employed. The electrode setup was the same as for DC polarization tests. The electrolyte used was a 3.5 wt. % NaCl solution. The exposed area of the sample was $1cm^2$. EIS determination was started

after 30 minutes of immersion of any sample in the electrolyte solution. Equivalent circuits were used to study the various electrochemical aspects of the coatings. Seven data points per decade and a frequency range from 10^5 - 10^{-2} Hz, with an alternating current (AC) voltage amplitude of ±10mV was used.
Energy dispersive x-ray spectroscopy (EDS) analysis was performed for the Ce-BTMS coating to provide an insight into the corrosion protection methodology of cerium ions. An FEI Helios NanoLab 600i machine with an accelerating voltage of 20kV was used.

3. Results

3.1. SEM analysis

The coating coverage and uniformity was determined by SEM analysis. The SEM micrographs for the three different coatings are presented in figure1.
Uniform, defect-free coatings are observed for all the three cases. Darker areas are regions with greater silane deposition [15]. Only very few randomly scattered pin holes are observed. For the APS coating dark islands surrounded by less darker regions can be observed. This can be attributed to a greater degree of condensation reaction occurring within the APS silane as well as greater degree of adsorption on Mg-containing particles [15]. The BTMS coating shows a uniform coating devoid of dark island-like formations seen for APS coating representing a greater degree of hydrolysis reaction leading to formation of metallosiloxane bonds and a lesser degree of self-condensation reaction. Even for the Ce-BTMS coating the surface shows overall uniformity indicating that the concentration of cerium ions used is blow the critical limit that can cause agglomeration and excess porosity.

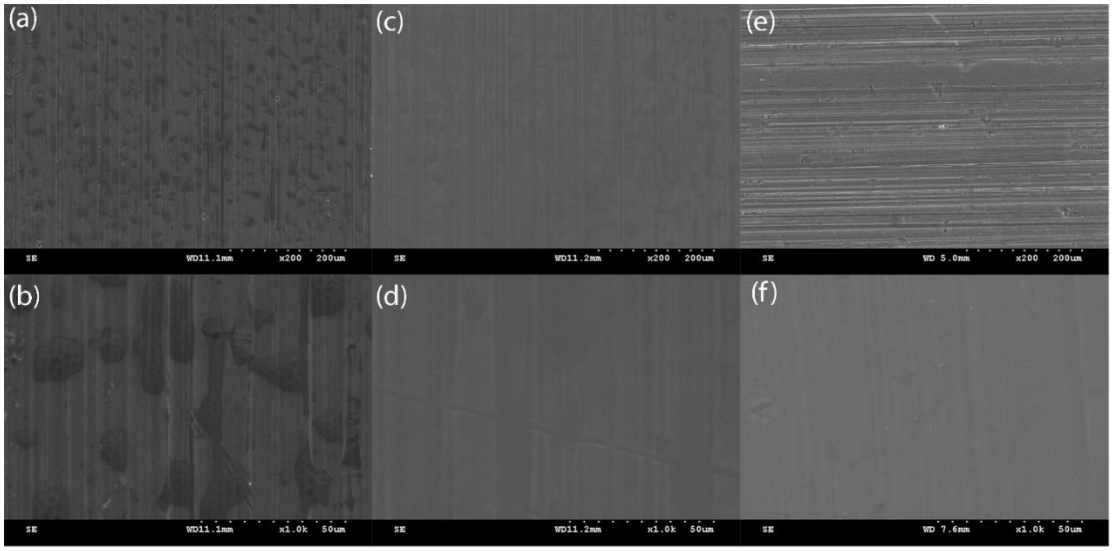

Figure 1. SEM micrographs of (a-b) APS (c-d) BTMS and (e-f) Ce-BTMS silane films

3.2. DC polarization

DC polarization tests were performed in 3.5 wt. % NaCl solution and the results are presented in figure 2.
The pure BTMS coating provides a much enhanced corrosion protection as compared to the APS coating which is evidenced by substantially reduced current densities for both anodic and cathodic parts of polarization curve as compared with the bare alloy. For the BTMS coating the current density is more than one order of magnitude lower than the uncoated sample. This shows the enhanced physical barrier properties of the BTMS as compared to the APS coating. The reduction in cathodic current densities can be explained as the blockage of some of the active cathodic sites by the silanes. The decrease in the anodic current density can be attributed to a decreased rate at which the corrosion products can migrate away from the initial pitting sites due to the formation of dense Al-O-Si interface [16]. For silane coated samples the corrosion products mainly intrude into the pores in the interfacial

layer leading to pore blockage. This effect leads to an increase in the coating resistance and has been further detailed by EIS analysis.

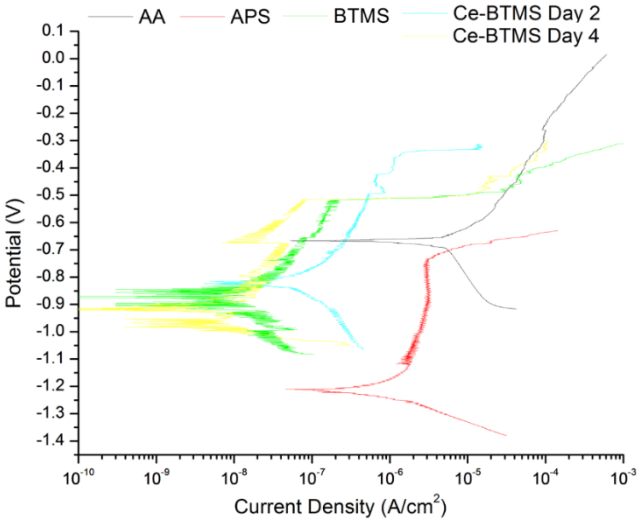

Figure 2. DC polarization curves of silanes at different immersion times

For the Ce-BTMS coating it can be seen that the decrease in anodic and cathodic current densities is virtually the same as un-doped BTMS even after two days of immersion. This shows that the chosen concentration of cerium ions is low enough as to not damage the physical barrier properties of the coating system by leading to an increased number of pin hole defects in the coating. It can also be seen that a further decrease in current densities is observed in the polarization curve conducted after four days of immersion. This decrease in current densities could be due to the deposition of cerium oxide/hydroxides at the sites of corrosion initiation. This phenomenon can be referred to as "active" corrosion protection, where the cerium ions from the coating migrate to corrosion pit initiation sites and deposit as oxide or hydroxides and retard the corrosion progress. This is shown by the shifting of Ecor towards more cathodic values as well as the emergence of a secondary peak around -1.0 V on the cathodic branch of polarization curve. Such a peak is generally observed for cerium coatings [17], which act as cathodic inhibitors. The emergence of this peak also evidences a chemical barrier rather than a simple physical barrier that is provided by the silanes.
The presence of such hydrated oxides of cerium along with the native aluminum oxide layer can lead to the formation of a barrier towards the flow of electrons. This can inhibit corrosion by reducing the rate of oxygen reduction. This process was further explored by EIS and EDS analysis.

3.3. EIS
Efficacy of the silane films was evaluated over a range of immersion period in 3.5 wt. % NaCl solution. figure 3-5 shows the Bode plots after various intervals of immersion. Symbols represent the measured data while the solid lines are the equivalent circuit fitting results.
EIS has been widely used to evaluate silane coatings, both doped and undoped, deposited on aluminum alloys. The Bode plots present a characteristic curve. At high frequencies between 10^5 and 10^2 Hz the impedance curve shows the resistive and capacitive contribution from the silane coatings. While at frequencies slightly lower than 102 Hz the intermediate oxide layer effects are observed. At lowest frequency the information from the corrosion processes characterized by polarization resistance and double layer capacitance can be obtained.

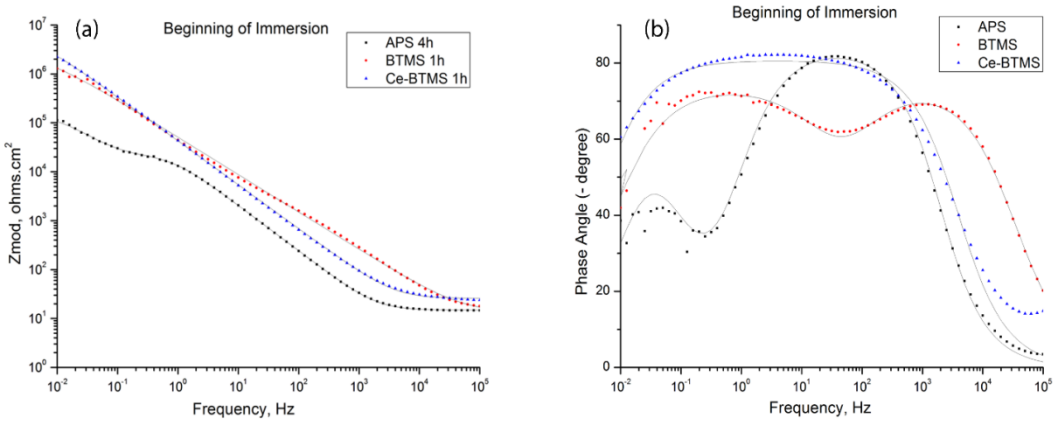

Figure 3. Bode plots at beginning of immersion

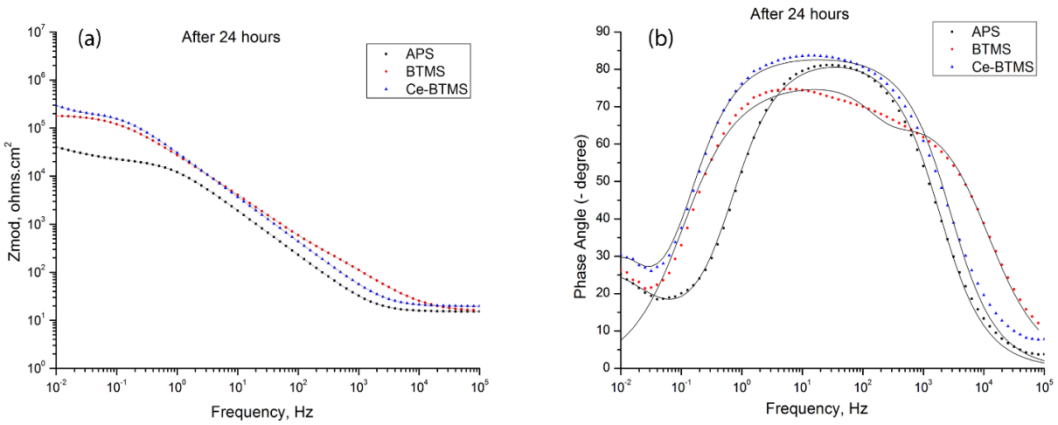

Figure 4. Bode plots after 24 hours of immersion

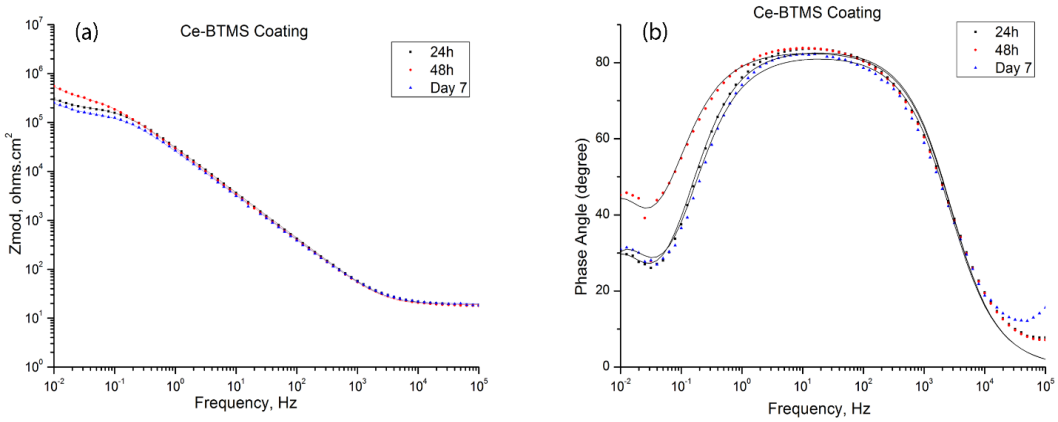

Figure 5. Bode plots for Ce-BTMS coating for prolonged immersion

Figure 3 shows the Bode plots of the silane coatings at the beginning of immersion period. APS shows lowest impedance value at the beginning of immersion along with lowest phase angles in the lower frequency region. Whereas the impedance and phase angle values obtained for un-doped BTMS in the high frequency region 10^3 to 10^5 are the highest indicating good barrier properties of the coating. These values decrease slightly in the lower frequency region. The highest impedance and phase angle values are shown by doped-BTMS sol-gel coating indicating excellent barrier resistance. The results are in keeping with those obtained from DC polarization study.

The Bode plots in figure 3 were obtained just after the start of immersion in the saline solution and already some signs of water permeation into the APS and BTMS coating are emerging. The Ce-BTMS

coating seems to be offering the best comparative retardation of water permeation in early stages of immersion.

After 24 hours of immersion it appears that the coatings are saturated with water resulting in decreased impedance values for all the coatings, as in figure 4. The barrier effectiveness of the BTMS coating decreases with values in the high frequency now close to those of Ce-BTMS coating. Even then BTMS coating seems to be faring better than the APS which could be due to the hydrophilic nature of amino functional group in the APS coating. For APS coating signs for initial corrosion are also emerging as evidenced by the appearance of a well-defined time constant in the lowest frequency range. For BTMS coatings although the time constant is not as well-defined as that for APS coating but initiation of pitting corrosion seems likely.

After 48 hours multiple barely visible pits can be observed for the APS coated sample and the values of impedance modulus fall to a low value of around $3x10^4$ ohms. This deterioration of coating could be due to the relatively weak interface formed by the APS coating due to its fewer hydrolysable groups and compounded by the aggressive uptake of water due to the hydrophilic functional group in its molecule. For the BTMS coating the impedance modulus values are nearly one decade higher than those for APS coating after 48 hours and the coating seems to hold its impedance values from 24 hours which could be due to the much slower permeation rate of water into the coating thus allowing the initial corrosion products to retard the pit from growing quickly. In contrast to both other coatings the Ce-BTMS coating shows nearly a four time increase in the impedance values from 24 hours to 48 hours. The values of impedance remain upwards that after 24 hours for more than 7 days of immersion, shown in figure 5. This self-healing property of the coating could be due to the formation of a passive cerium hydroxide layer where cerium ions leach out from the coating in the vicinity of the pitting site and deposit over the defect. The probable mechanism involved has been studied by various authors [14], [18]. Succinctly, in a chloride rich environment S-phase intermetallics having composition Al2CuMg are main culprits for corrosion of 2024 aluminum alloy. These intermetallics can act as effective cathodes where oxygen reduction can occur via four-electron step or two-electron step resulting in hydroxide ions and peroxide formation:

$$O_2 + H_2O + 4e^- \rightarrow 4OH^- \quad (1)$$

$$O_2 + 2H_2O + 2e^- \rightarrow H_2O_2 + 2OH^- \quad (2)$$

A cathodic reaction can take place resulting in the formation of highly insoluble hydroxides as:

$$Ce^{3+} + 3OH^- \rightarrow Ce(OH)_3 \quad (3)$$

Alternatively Ce^{3+} ions can get oxidized by peroxide to Ce^{4+} state as:

$$Ce^{3+} + \frac{1}{2}H_2O_2 + 3OH^- \rightarrow Ce(OH)_4 \quad (4)$$

$$Ce(OH)_4 \rightarrow CeO_2.2H_2O \quad (5)$$

Thus, if a sufficient concentration of cerium ions is available the cathodic process can be greatly retarded by formation of these insoluble hydroxide deposits.

For continued immersion beyond 48 hours for the APS coated sample it can be seen that the impedance values remain nearly constant and pitting progresses at a steady rate. Beyond 96 hours the pits become more easily visible and a very slight increase in impedance value is observed which could be due to the presence of excess corrosion products in and around the pits which can lead to some barrier protection against the corrosion progression.

For the BTMS coating the impedance modulus values fall progressively over the first 7 days of immersion at which point a couple of pits become visible. Upon continued immersion beyond this time a similar phenomenon of pit blockage by excess corrosion product is observed resulting in a slight increase in impedance values to day 11 when the experiment was stopped. For the Ce-BTMS coating the pits only become visible after 10 days of immersion. But the rate of pit progression

remains very slow as impedance values after 16 days which are nearly identical to those observed after 10 days.
Equivalent circuits can be used to gather more insight about the influence of various parameters on the sol-gel coated samples. The equivalent circuits which were used to represent various stages during EIS immersion study are shown in figure 6.

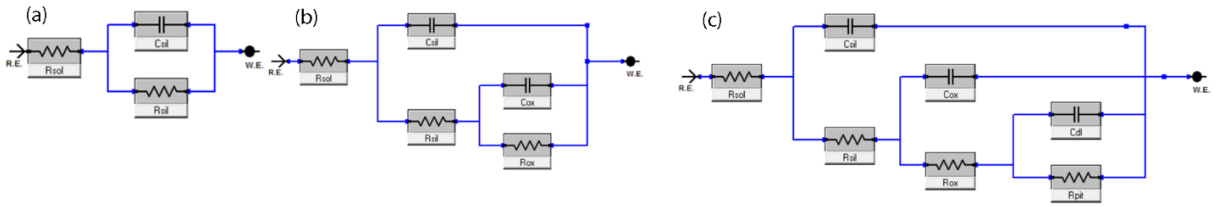

Figure 6. Equivalent circuits (a) beginning of immersion (b) oxide layer resistance (c) on-set of corrosion

In the above circuits Rsol is the solution resistance, Rsil is resistance of the silane layer, Rox is the oxide resistance and Rpit is the pitting or polarization resistance. Csil, Cox and Cdl are silane, oxide and double layer capacitances respectively. Capacitors were replaced by constant phase elements (CPE) as the phase angles were different from -90^{o}, which is a necessary condition for ideal capacitor. The impedance of CPE can be given by [4]:

$$Z_{CPE} = \left(1/Y\right)/\left(jw\right)^{a} \quad (6)$$

The parameter 'Y' corresponds to pseudo-capacitance, while 'a' relates the systems homogeneity. If the values of a =1 and Y = C, this condition would represent a capacitor, whereas the value of a will be less than 1 for a CPE.
The equivalent circuits were used to model different stages of immersion. Circuit (a) is used at the beginning of immersion and gives only the capacitive and resistive response of the coating along with solution resistance. The circuit (b) incorporates the resistive and capacitive responses for the native oxide layer on aluminum alloy as well as the Al-O-Si layer that can form between the silane and the substrate. In circuit (c) double layer capacitance and pitting resistance are incorporated to model the influences of pitting phenomenon. The chi-squared error values were less than 10^{-3} for all fittings.
The low concentration on cerium was chosen to ensure that the coating uniformity is not disrupted by resulting in pin holes or agglomeration of cerium ions. The SEM results show a uniform coating free of agglomerates and a very few scattered pin holes. At the beginning of immersion, figure 7, the coating resistances of BTMS and Ce-BTMS coatings are very close to one another. But, after nearly 24 hours of immersion Ce-BTMS coating shows higher values of resistance and after 48 hours the difference is much more pronounced. The higher R(sil) values for Ce-BTMS coating could be due to pore blocking action of cerium ions or the passivation of pit initiation sites by cerium ions which is more evident around 24 to 48 hours of immersion. This could presumably lead to a slower degradation of coating as the rate at which corrosion products are generated is much slower. BTMS coating loses most of its protective action around 168 hours of immersion and values fall to the range of 10^{1} whereas for Ce-BTMS coating the coating only reaches this stage after 216 hours of immersion. For the APS coating the barrier properties are not as effective with coating resistance falling sharply during 24 hours to 48 hours. This can be attributed to the hydrophilic nature of its functional group or upside down deposition [15] of its molecules which can adversely affect its protective nature. The values fall to around 10^{2}-10^{1} range after only 48 hours and maintain these to around 96 hour mark, after which the values rise to around 10^{3} which can be due to a large build-up of corrosive products. This phenomenon of increase in resistance due to corrosion products can also be seen for BTMS coating but is less pronounced probably due to a smaller quantity of corrosion products. Whereas for the Ce-BTMS this phenomenon is almost negligible from 240 to 384 hours indicating only a very slow corrosion rate where the corrosion products might have enough time to diffuse a little further away for

the corrosion site. But we can presume that if the immersion is continued a similar increase in resistance can be observed due to eventual build up corrosion products.

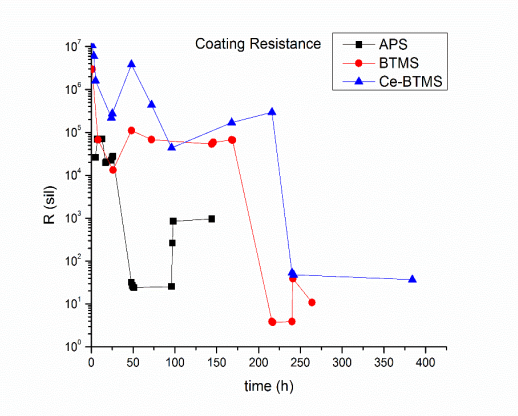

Figure 7. Silane film resistance with immersion time

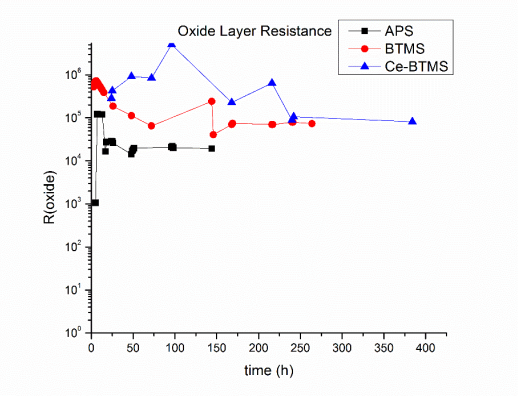

Figure 8. Oxide layer resistance with immersion time

The oxide layer resistance values shown in figure 8, for APS coating are nearly one decade and two decade lower than those for BTMS and Ce-BTMS coating. This most likely occurs due to the low number of interfacial bonds that APS can form resulting is a weaker interface. For the BTMS coating a denser interface can formed due to the presence of more hydrolysable groups present in its structure. The oxide layer only registers a very slow decrease in its resistive values. For the Ce-BTMS coating the oxide layer resistance values show an initial increase in contrast to the other two coatings. This can be explained by considering the corrosion initial phenomenon for aluminum alloys. In aluminum alloys like 2024 the oxide layer is much thinner over the intermetallic phases and due to the electronegativity difference between these phases and the surrounding aluminum phase corrosion will initiate at these sites [3], [15]. For the Ce-BTMS coating not only is a denser interface formed due to more hydrolysable groups, as soon as pit initiation occurs a non-soluble cerium hydroxide layer is formed at these points. Thus, in a matter of speaking, repairing the oxide layer. This phenomenon is easily observable between 24 to 96 hours where resistance values for Ce-BTMS coating are more than a decade higher than those observed for un-doped BTMS coating. Eventually after 240 hours both the BTMS coatings approach similar values which points that the positive influence of cerium ions has disappeared. This points towards one of the key areas which needs to be optimized in future studies, where the release of dopant ions has to be prolonged or a mechanism for preparing a re-loadable coating have to be investigated.

3.4. Corrosion Process

Polarization resistance (Rpit) can be used to evaluate the rate of corrosion processes. The polarization resistance for the coatings is given in Table I.

Table I. Polarization resistance with immersion time.

APS Coating		BTMS Coating		Ce-BTMS Coating	
Time (h)	R(pit) ohms cm^2	Time (h)	R(pit) ohms cm^2	Time (h)	R(pit) ohms cm^2
48	4.28E+04	216	7.41E+04	240	1.18E+05
96	2.51E+04	240	8.81E+04	384	9.37E+04
144	1.79E+03	264	9.39E+04	-	-

The APS coating only provides a fair protection with polarization resistance values in the range of 10^4 after 48 hours of immersion. These values fall to 10^3 after 144 hours of immersion and large corrosion can be observed on the coated sample. The low polarization resistance values are due to the poor barrier properties of the coating. The un-doped BTMS coating offers a much improved polarization resistance with values around $7x10^4$ after 216 hours of immersion and remain in this range even when the immersion time increases to 264 hours. The Ce-BTMS offers the highest polarization resistance values with the third time constant related to pitting appearing only around 240 hours of immersion and values of about $1x10^5$. Even with continued immersion these values are maintained and only after 384 hours the values show a small decrease and falling to around $9x10^4$. The improved polarization resistance values for the BTMS coating are due to much better barrier properties as well as denser interface formation. For the Ce-BTMS coating these values are further enhanced and show decrease only when the cerium ions are released from the coating and the inhibition by cerium ions is discontinued.

3.5. EDS Analysis

In order to ascertain that cerium is present inside the pits an EDS analysis, shown in figure 9, was performed after 4-7 days of immersion in 3.5 wt. % NaCl solution. EDS analysis was also carried out at multiple points for the coating that has not been immersed in NaCl solution.

For the coating that has not been immersed in NaCl solution a few of the tested regions did not show a signal for cerium which could be either due to the non-uniform distribution of the cerium in the coating or due to the very low concentration of the cerium in the final coating. However, a signal for cerium was detected in most tested regions with a maximum of around 0.34 wt. % (0.06 atomic %). But in case of the coating that was immersed for 7 days in NaCl solution, a signal for cerium is always detected in the area of pit. For a relatively smaller pit the signal strength of cerium is higher at 0.65 wt. % (0.1 atomic %) whereas for a larger pit the detected value is lower at 0.22 wt. % (0.03 atomic %). The growth of the pit with time could probably lead to removal of cerium hydroxide deposits from the pit or it possible that the region around the pit initially had a lower concentration of cerium due to non-uniform distribution that the cerium concentration in the pit was not sufficient to actively passivate the pit and thus the pit grew more than the other pit as well as has a lower final cerium concentration. These assumptions also fit the smaller pit where the smaller pit growth could be either due to a larger concentration of cerium and thus a better active protection or the fact that this pit initiated at a later stage and thus has smaller size and higher concentration of cerium. In either case, EDS analysis supports the claim that cerium ions deposit at pit initiation sites and provide an active corrosion protection at least for a moderate time of immersion.

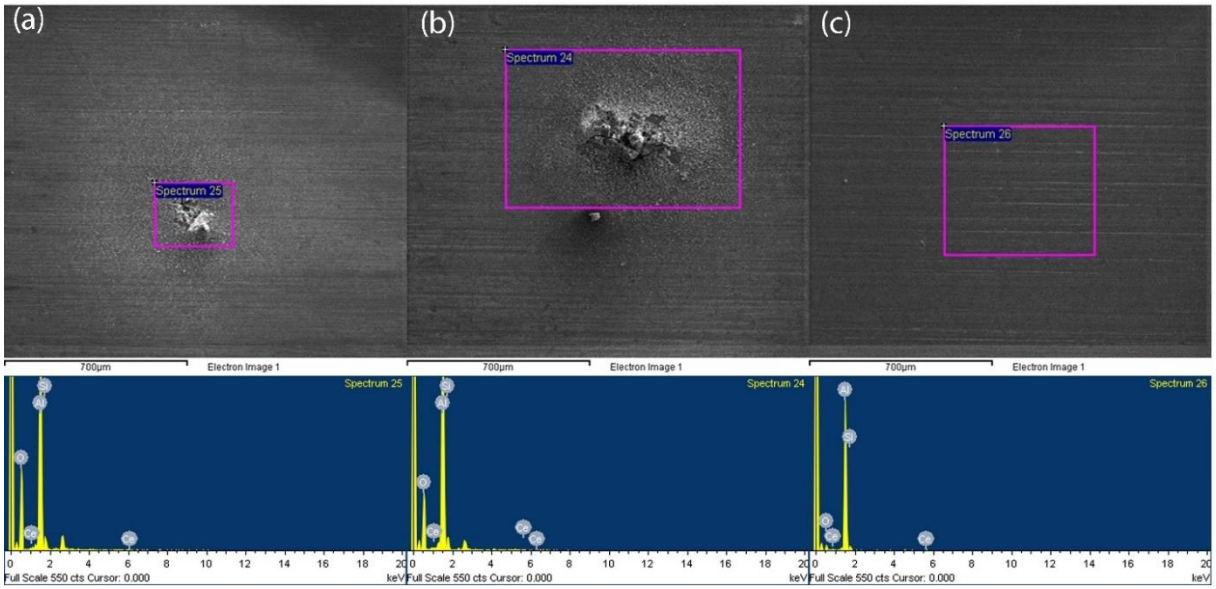

Figure 9. EDS micrographs (a) small pit (b) larger pit (c) un-immersed coating area

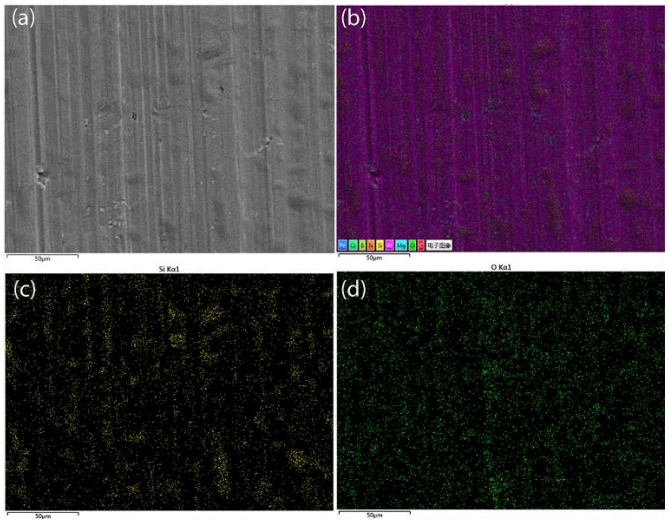

Figure 10. EDS mapping representing self-condensation of APS silane (a) optical (b) all major elements (c) Si (d) O mapping

Figure 10 is an EDS mapping of APS silane film. The mapping again shown island-like morphology for the APS. Figure 10(c) provides evidence that these islands are agglomerates of silicon, which result from the excessive self-condensation of the silane. This non-uniformity exhibited by APS is one of the causes of its poorer performance.

4. Conclusion

Coating and metal/interface properties of sol-gel pre-treatments can be studied by using EIS method for aluminum alloys. Three different types of coatings were evaluated for their corrosion protection in 3.5 wt. % NaCl solution.

For the APS coating, a slightly hydrophilic functional group together with fewer number of hydrolysable groups leads a less cross-linked Si-O-Si barrier layer and a less dense interface between the silane and alloy. These lead to only a fair improvement in the corrosion resistance of the substrate. The use of BTMS provides much improved protection due to higher number of hydrolysable groups resulting in a highly cross-linked barrier layer and a dense Al-O-Si interface.

The BTMS coating alone can however only provide a physical barrier against the corrosive medium and thus only passive protection. A small amount of cerium ions were introduced into the BTMS

coating to investigate their influence on the pre-treatment. SEM analysis reveals that the cerium salt concentration is low enough to not disturb the uniformity and homogeneity of the coating. Linear polarization tests reveal the enhanced corrosion protection provided by BTMS and Ce-BTMS coatings as compared with APS coating. Evidence for chemical protection provided by Ce-BTMS coating is provided by a secondary peak in the cathodic branch of tafel curve. EIS testing along with EDS analysis reveals that the cerium ions can deposits at sites of pit initiation as insoluble cerium hydroxide deposits and thus provide an enhanced and active corrosion protection to the AA2024 substrate.
This active protection effect however diminishes with continued immersion and methods to incorporate greater concentration of cerium ions without disturbing the morphology of the coating and providing a prolonged release of inhibitor ions needs to be investigated.

5. References

[1] M. Kendig, S. Jeanjaquet and R. Addison et al., "Role of hexavalent chromium in the inhibition of corrosion of aluminum alloys," Surface and Coatings Technology, vol. 140, no. 1, pp. 58-66, May 2001.
[2] J. Zhao, L. Xia and A. Sehgal et al., "Effects of chromate and chromate conversion coatings on corrosion of aluminum alloy 2024-T3," Surface and Coatings Technology, vol. 140, no. 1, pp. 51-57, May 2001.
[3] D. Zhu and W. J. van Ooij, "Corrosion protection of AA 2024-T3 by bis-[3-(triethoxysilyl)propyl]tetrasulfide in neutral sodium chloride solution. Part 1: corrosion of AA 2024-T3," Corrosion Science, vol. 45, no. 10, pp. 2163-2175, Oct. 2003.
[4] N. C. Rosero-Navarro and S. A. Pellice, A. Durán et al., "Effects of Ce-containing sol–gel coatings reinforced with SiO2 nanoparticles on the protection of AA2024," Corrosion Science, vol. 50, no. 5, pp. 1283-1291, May 2008.
[5] A. M. Cabral, R. G. Duarte and M. F. Montemor et al., "A comparative study on the corrosion resistance of AA2024-T3 substrates pre-treated with different silane solutions: Composition of the films formed," Progress in Organic Coatings, vol. 54, no. 4, pp. 322-331, Dec. 2005.
[6] A. P. More and S. T. Mhaske, "Chemical Modification of Silane-Based Coating with Inhibitor for Anticorrosive Application," Arabian Journal for Science and Engineering, vol. 41, no. 6, pp. 2239-2248, June 2016.
[7] J. Mosa, N. C. Rosero-Navarro and M. Aparicio, "Active corrosion inhibition of mild steel by environmentally-friendly Ce-doped organic-inorganic sol-gel coatings," RSC Advances, vol. 6, no. 46, pp. 39577-39586, April 2016.
[8] M. L. Zheludkevich, R. Serra and M. F. Montemor et al., "Nanostructured sol–gel coatings doped with cerium nitrate as pre-treatments for AA2024-T3: Corrosion protection performance," Electrochimica Acta, vol. 51, no. 2, pp. 208-217, Oct. 2005.
[9] A. Ahmadi, B. Ramezanzadeh and M. Mahdavian, "Hybrid silane coating reinforced with silanized graphene oxide nanosheets with improved corrosion protective performance," RSC Advances, vol. 6, no. 59, pp. 54102-54112, May 2016.
[10] L. Calabrese, L. Bonaccorsi and A. Caprì et al., "Assessment of hydrophobic and anticorrosion properties of composite silane–zeolite coatings on aluminum substrate," Journal of Coatings Technology and Research, vol. 13, no. 2, pp. 287-297, March 2016.
[11] M. Gharagozlou, R. Naderi and Z. Baradaran, "Effect of synthesized NiFe2O4-silica nanocomposite on the performance of an ecofriendly silane sol–gel coating," Progress in Organic Coatings, vol. 90, pp. 407-413, Jan. 2016.
[12] L. Lei, J. Shi and X. Wang et al., "Microstructure and electrochemical behavior of cerium conversion coating modified with silane agent on magnesium substrates," Applied Surface Science, vol. 376, pp. 161-171, July 2016.
[13] C. F. Malfatti, T. L. Menezes and C. Radtke et al., "The influence of cerium ion concentrations on the characteristics of hybrid films obtained on AA2024-T3 aluminum alloy," Materials and Corrosion, vol. 63, no. 9, pp. 819-827, Sep. 2012.
[14] R. Zandi Zand, V. Flexer and M. De Keersmaecker et al., "Self-healing silane coatings of cerium salt activated nanoparticles," Materials and Corrosion, vol. 67, no. 7, pp. 693-701, July 2016.

[15] D. Susac, X. Sun and K. A. R. Mitchell, "Adsorption of BTSE and gamma-APS organosilanes on different microstructural regions of 2024-T3 aluminum alloy," Applied Surface Science, vol. 207, no. 1-4, pp. 40-50, Feb. 2003.
[16] D. Zhu and W. J. van Ooij, "Corrosion protection of AA 2024-T3 by bis-[3-(triethoxysilyl)propyl]tetrasulfide in sodium chloride solution.: Part 2: mechanism for corrosion protection," Corrosion Science, vol. 45, no. 10, pp. 2177-2197, Oct. 2003.
[17] H. D. Johansen, C. M. A. Brett and A. J. Motheo, "Corrosion protection of aluminium alloy by cerium conversion and conducting polymer duplex coatings," Corrosion Science, vol. 63, pp. 342-350, Oct. 2012.
[18] K. A. Yasakau, M. L. Zheludkevich and O. V. Karavai et al., "Influence of inhibitor addition on the corrosion protection performance of sol–gel coatings on AA2024," Progress in Organic Coatings, vol. 63, no. 3, pp. 352-361, Oct. 2008.

Acknowledgments
The authors acknowledge financial support by the National Natural Science Foundation (Grant No. 51272055 and 51501050).